NASA Technical Memorandum 82996

Experimental Investigation of the Vaporous/Gaseous Cavity Characteristics of an Eccentric Journal Bearing

M. J. Braun
University of Akron
Akron, Ohio

and

R. C. Hendricks
Lewis Research Center
Cleveland, Ohio

Prepared for the
Joint Lubrication Conference
cosponsored by the American Society of Mechanical Engineers
and the American Society of Lubrication Engineers
Washington, D.C., October 4-6, 1982

NASA

An Experimental Investigation of the Vaporous/Gaseous Cavity Characteristics of an Eccentric Journal Bearing

M. J. BRAUN
University of Akron, Akron, Ohio 44325
R. C. HENDRICKS
NASA-Lewis Research Center, Cleveland, Ohio 44135

This paper describes the experimental pressure and temperature results obtained when rotating a shaft in an eccentric lucite casing at velocities ranging from 209 to 628 rad/s (2000 to 6000 rpm). The results are presented in terms of three-dimensional plots and contour maps. Photographic evidence is presented to illustrate how the downstream and upstream regions of the cavity develop and evolve into the well-known finger patterns. A comparison between pressure and temperature profiles in air-saturated oil and carbon dioxide-saturated oil is presented; the origin and nature of the gases contained in the cavity are discussed. Three analytical models (Swift-Stieber, separation, Floberg) predicting the formation of the cavitation zone are presented and evaluated in light of the experimental results. A motion-picture supplement depicting these results is available upon request.

INTRODUCTION

Cavitation Boundary Conditions—Short Theory Review

The basic theory of hydrodynamic lubrication was set in 1886 when Reynolds, (*1*), derived the differential formulation for pressure buildup in a thin lubricating film. The equation

$$\frac{\partial}{\partial x}\left(\frac{\rho h^3}{12\eta}\frac{\partial P}{\partial x}\right)+\frac{\partial}{\partial y}\left(\frac{\rho h^3}{12}\frac{\partial P}{\partial y}\right)=\frac{\partial}{\partial x}\left[\frac{\rho(u_1+u_2)}{2}h\right]+\frac{\partial(\rho h)}{\partial t} \quad [1]$$

can accurately describe the fluid film pressure distributions—under loading—in the convergent portion and a limited part of the unruptured divergent film where the pressure $p>0$. In 1904, Sommerfeld (*2*) published his now-famous solution of the pressure distribution for an infinitely wide, 360°, full-clearance oil film journal bearing. He recognized cavitation as a limitation of his theory and predicted the existence of subatmospheric pressures in the diverging section of the bearing surfaces, as shown in Fig. 1(A). Gumbel (*3*) made the first attempt to model the film rupture, followed by Swift (*4*) and Stieber (*5*). All three authors neglected the subatmospheric pressure loop. Swift and Stieber solved Eq. [1], using Eq. [2] for the inception of the cavitation region,

$$\frac{\partial P}{\partial x}=0 \qquad P=P_{cavity}=P_{atm} \quad [2]$$

This film rupture condition yields a pressure distribution as the one shown in Fig. 1(B). Hopkins (*6*) in 1957, Bretherton (*7*), Taylor (*8*) in 1960, and Coyne and Elrod (*9*), in 1970 observed the experimental occurance of the subcavity

NOMENCLATURE

- h = clearance height
- n = number of moles
- P = pressure
- q = heat flux
- R = gas constant
- $R_{1,2}$ = radius of curvature
- T = temperature
- t = time
- u = velocity
- u_1 = surface velocity, journal
- u_2 = surface velocity, housing
- V = volume
- x, θ = coordinate in direction of rotating
- y, Z = coordinates parallel to shaft centerline
- θ = circumferential coordinate
- η = viscosity
- ρ = density
- σ = surface tension

Subscripts

- f = film
- g = gas
- sc = subcavity
- v = vapor

Presented at the ASLE/ASME Lubrication Conference, Washington, D.C., October 5–7, 1981

pressure loop in bearings and suggested a mechanism whereby the flow separation effect may be instrumental in the film rupture. Separation would occur when

$$\frac{\partial u}{\partial y} = 0 \qquad [3]$$

takes place, a condition equivalent to the inception of secondary flows, causing a flow reversal region where the dissolved gases can congregate. At the cavitation boundary, this implies an adverse pressure gradient given by

$$\frac{\partial P}{\partial x} = \frac{2\eta U_1}{h^2} \qquad [4]$$

The separation theory results in a pressure distribution profile which can accommodate the subatmospheric pressures, Fig. 1(C). While the separation theory (*7*)–(*10*) considers that the lubricant moves under and/or over the cavity, Fig. 2(A), Floberg (*11*), (*12*) postulates that: (a) the flow is carried between the cavities, Fig. 2(B), and (b) no net mass flow penetrates into the cavity. In the light of (a) and (b), Floberg derives a boundary condition which connects the oil film to the cavitation zone.

$$\frac{\partial P}{\partial x} - \frac{\partial P}{\partial y}\frac{dx}{dy} = \frac{6\eta\,(U_1 + U_2)}{h^2} \qquad [5]$$

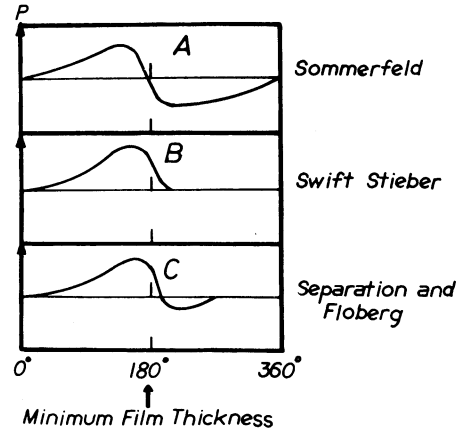

Fig. 1—Three possible pressure distribution configurations for different cavitation boundary conditions.

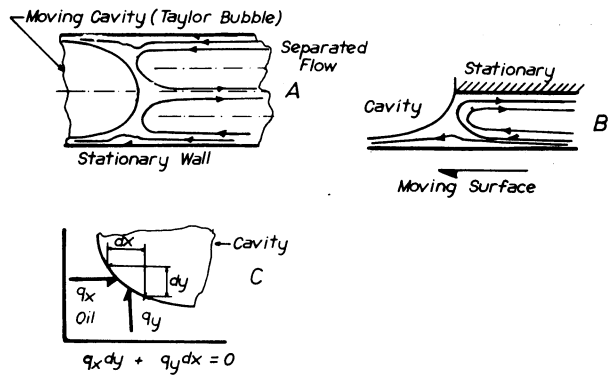

Fig. 2—Physical conditions leading to the apparition of the gaseous cavity and pressures below atmospheric; separation versus Floberg case.

Pseudo, Gaseous, and Vaporous Cavitation: Some New Arguments

The content of the cavitation bubble has been a matter of argument ever since Reynolds (*1*) derived the basic equation of lubrication theory. Hydrocarbon vapor versus liberation of dissolved gases—that is the question! Today, researchers are still trying to elucidate the problem.

One can distinguish between three types of mechanisms which can create and cause a bubble to grow.

Let us assume that there exists a homogeneous film mixture of oil and dissolved gases at a given pressure P_f.

(a) If, suddenly, the pressure is reduced to P_g, but remains larger than P_v, the dissolved gas nuclei will merge into a separate gaseous phase and, at a critical cluster radius*, rupture the homogeneity of the oil film. This is the essence of gaseous cavitation. The lowest pressure the oil film can sustain depends on mass fraction, solubility, and type of gases dissolved in the oil. The more gas in the oil, the closer the cavity pressure will be to the atmospheric pressure and the sooner the rupture of oil film will occur.

The cavity pressure will represent the pressure drop which the oil can withstand at the moment before the film is broken due to the release of dissolved gases. This pressure drop has to be equivalent with the maximum surface tension, σ, which the liquid can tolerate. For a bubble of arbitrary shape, the equation connecting the film pressure, P_f, the cavity pressure, P_c, and the surface tension (tensile stress) is

$$P_c - P_f = \sigma\left(\frac{1}{R_1} + \frac{1}{R_2}\right) \qquad [6]$$

In Eq. [6], the cavity pressure is, in most cases, the sum of the vapor pressure and the pressure of the noncondensable impurities,

$$P_c = P_v + P_g \qquad [7]$$

By introducing Eq. [7] into Eq. [6], one obtains

$$P_v + P_g - P_f = \sigma\left(\frac{1}{R_1} + \frac{1}{R_2}\right) \qquad [8]$$

which physically relates P_v, P_g, and P_f to the surface tension σ. Under the conditions described previously at (a), Eq. [8] becomes

$$P_g - P_f = \sigma\left(\frac{1}{R_1} + \frac{1}{R_2}\right) \qquad [9]$$

and gaseous cavitation ensues as a function of the surface tension, film pressure, and geometry.

(b) If the pressure is lowered to $P < P_v$, volatile hydrocarbon nuclei can be engendered by nucleation sites at the surfaces (akin to nucleate boiling) or by impurities existing in the fluid. Upon nucleation, they will either form a new cavity or be released into an existing gaseous cavity, forming

* vapor/gas release is often triggered by sites on the boundaries, following the active site criteria of Hsu.

a mixture of dissolved gases and vapors. For the case that no noncondensable impurities are present in the oil and the film thickness is sufficiently large for bubble formation, the lowest pressure in the film just before rupture will be the oil-vapor pressure. Equation [6] becomes

$$P_v - P_f = \sigma \left(\frac{1}{R_1} + \frac{1}{R_2}\right) \qquad [10]$$

Both the mixture and the separate components are considered perfect gases, and, according to Dalton's law, one can write for the mixture

$$\begin{aligned} P_c V &= nRT \\ n &= n_v + n_g \end{aligned} \qquad [11]$$

and for the components

$$\begin{aligned} P_v V &= n_v RT \\ P_g V &= n_g RT \end{aligned} \qquad [12]$$

In order to determine the ratio of partial pressures

$$\frac{P_v}{P_g} = \frac{n_v}{n_g} \qquad [13]$$

one has to know from the onset the molar ratio of the dissolved gases, volatility, and concentrations of hydrocarbons in the oil and their respective vapor pressures. It is our opinion that only in the light of the analysis of Eq. [10]–[12], can one begin to decide whether vaporous or gaseous cavitation has occurred. Quantitative arguments supporting the thesis of the largely gaseous (N_2, O_2, CO_2 i.e. air) nature of the cavity at the onset of formation are presented in the Appendix.

(c) Finally, the so-called pseudocavitation can occur when the size of the bubble changes due to a variation of P_f rather than an adiabatic and isothermal mass exchange from the oil to the cavity. If the mass stays constant, for a bubble of arbitrary shape,

$$V_i \rho_i = V \rho \qquad [14]$$

Considering that for an adiabatic or isothermal transformation

$$\frac{P_{c,i}}{(\rho_{c,i})^m} = \frac{P_c}{(\rho_c)^m} \; ; \; m = 1,k \qquad [15]$$

and that $R_1 = R_2$, Eq. [6] becomes between initial and final state

$$\left.\begin{aligned} P_{c,i} - P_{f,i} &= 2\sigma/R_i \\ P_c - P_f &= 2\sigma/R \end{aligned}\right\} \qquad [16]$$

and one can relate the film pressure to the cavity pressure by

$$\frac{P_f}{P_c} = 1 - \frac{1}{P_c}\left(\frac{P_c}{P_{c,i}}\right)^{1/3m} \frac{2\sigma}{R_i} \; ; \; m = 1,k \qquad [17]$$

where P_c is given by Eq. [7].

If one knows the oil molar composition, phase diagrams, and surface tension, one can determine the radius at which gaseous cavitation will start for a given film pressure. The curves of Fig. 13 and Table 1, Appendix, indicate the content of the cavity zone. While Eq. [16] gives for a combination (P_c, P_f) the radius at which cavitation can start, Eq. [17] shows that for an adiabatic or isothermal transformation, what may seem as an increase/decrease in the mass amount of the gaseous phase may, in reality, be an illusion due to the change in P_c and P_f.

To further elucidate the question of the cavity content, one has to also consider the criteria put forth by thermal bubble nucleation theory. According to Hsu (*14*) and Hsu and Graham (*15*) for a surface pit of radius R_c a superheat

$$T_b - T_{sat} = \frac{2\sigma T_{sat}}{C_2 R_c h_{fg} \rho_v} \qquad [18]$$

is necessary to create and sustain a vapor bubble. Bergles and Rohsenow (*16*) have proposed an expression for the heat flux which would generate vapor bubble inception,

$$q = AP^a \, (T_w - T_{sat})^{b/p^c} \qquad [19]$$

where A, a, b, c are constants to be determined experimentally. It thus becomes apparent, from the thermal viewpoint, that the generation of vapor in the cavity is contingent upon the fulfilment of a given set of pressures, temperatures, and heat fluxes as Eq. [18] and [19] show. Unless such conditions are respected, it is very probable that in case of film rupture, what we witness is gaseous cavitation or pseudocavitation (see also Appendix).

Jacobsen and Hamrock (*17*) report that for a journal and housing with controlled eccentric motion, the content of the fern-leaf structure associated with film rupture is vaporous. It is important that great care should be exerted in differentiating and identifying the various types of cavitation mechanisms.

SCOPE

This paper has as the main objective to present and explain experimental data concerning the pressure and temperatures characterizing the behavior of the bearing gap film when operating in the fully flooded mode. The data obtained are of significance for both seal and bearing technology.

Together with the photographic data detailing the start-up and steady-state regimes of the journal, we have obtained for the first time (to the best of our knowledge) three-parameter (3-D) digitized images of the temperature and pressure envelopes associated with both the full oil film and gaseous and/or vaporous (cavitation) zones. The tests have been run using, first, and oil with dissolved air at 0.034 – 0.055

MPa (5–8 psia) pressure, and then, for purposes of comparison, with same oil having carbon-dioxide dissolved under a pressure of approximately 0.117 MPa (17 psia).

A discussion of the experimental method and interpretation of two- and three-dimensional graphical data in light of existing theories concludes a portion of the work which represents the first part of a two-part paper; the second part to appear at a later date, will address the theoretical modeling of these experimental data.

A motion-picture supplement was made to illustrate the effects of axial and peripheral pressure, temperature, and visual void characteristics of the rotating journal at a fixed eccentricity at 2000, 4000, and 6000 rpm with cover gas pressures of air and carbon dioxide. The motion-picture supplement is available on loan from the Lewis Research Center Photographic Branch, (C-307).

EXPERIMENTAL EVIDENCE

The Experimental Facility

A schematic of the test section and oil flow diagram of the experimental rig is shown in Fig. 3. The detail "B" presents a sketch of the temperature-pressure transducer (TPT) used in the experiment. The test section is formed out of a journal 50.8 mm in diameter with an L/D ratio of 0.75 which is rotated by a spindle whose velocity can be varied from 193 to 1047 rad/s (1843 to 10 000 rpm). The eccentricity between the journal and the housing centerline was fixed at 0.4 with a minimum clearance of 0.00684 mm (*13*), located approximately 70° from the bottom of the configuration. The journal was enclosed by an acrylic transparent housing which was connected to a motor which in turn permitted a 360° rotation of the housing at low but variable speeds. In turn, the housing-motor configuration was mounted on a motorized linear slide which allowed the axial displacement of the housing, as shown in Fig. 3.

To accurately follow and record the position of the TPT, an electronic linear and angular indexing system was used in conjunction with two x-y plotters, recording concomitantly both pressures and temperatures at specific locations. The turbine flowmeters FM1 and FM2 located on each of the oil exit lines and the accompanying valves V1 and V2 were used to measure and control the oil flow on each side of the submerged rotating journal. The temperature at the test section oil inlet line was controlled by means of the water-cooled heat exchanger, HE. A thermocouple located at the heat exchanger exit measured the temperature of the oil feeding the test section. The oil was circulated by means of a gear oil pump provided with a bypass circuit used to control the test section oil mass flow and pressure.

The Experimental Procedure

Prior to data taking, oil was pumped with the bypass fully open to flood and slightly pressurize the test section until all the visible air bubbles were eliminated from the oil contained within the transparent reservoir. Special attention was given to the elimination of air bubbles in and around the TPT access orifice. The pressure in the test section was regulated by means of the valves V1 and V2 and the pump bypass valve V3. The next step was to start the oil submerged journal and bring it to the rotational speed for which the experiment was planned (2000, 4000, or 6000 rpm). After the test regime speed was reached, the test section oil inlet temperature was allowed to stabilize to a steady-state value. Then the mechanized TPT would perform sequential axial or circumferential sweeps with the

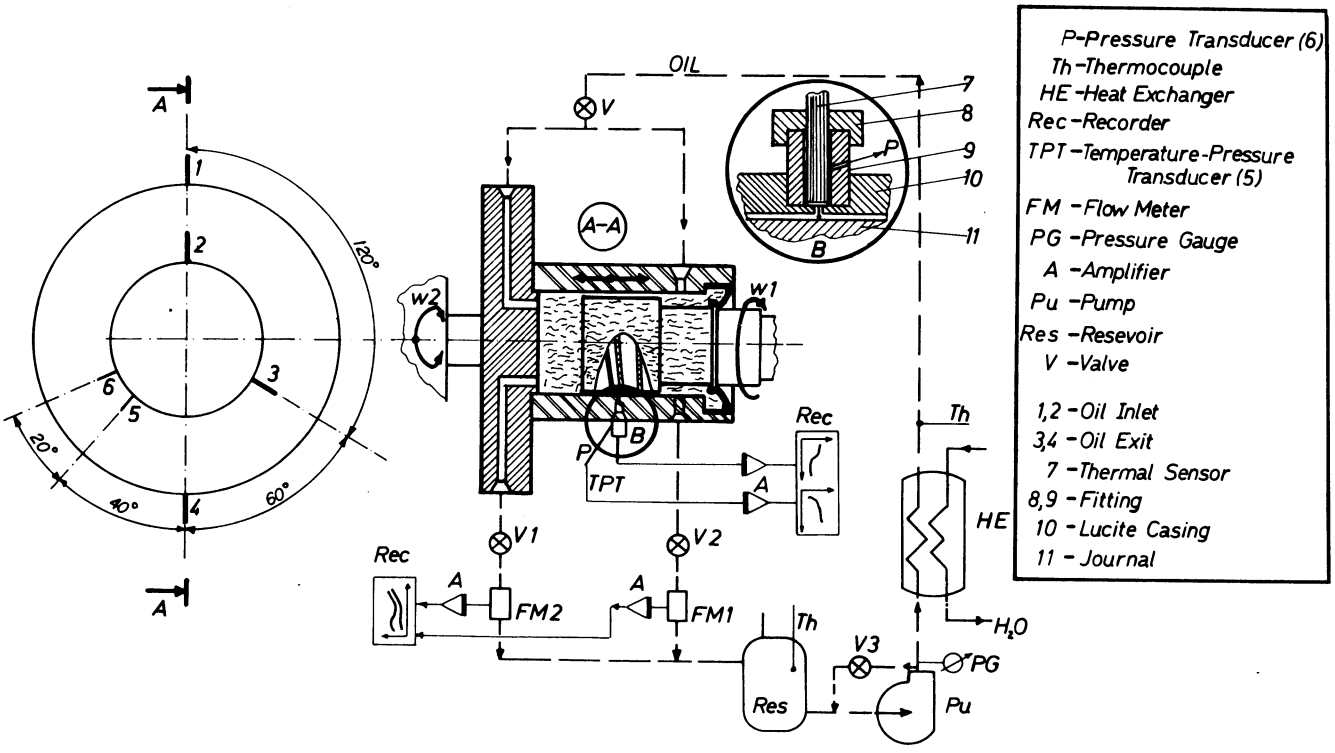

Fig. 3—Experimental facility schematic

pressure and temperature recorded concurrently on the x-y plotters. The behavior of the oil mass flows through FM1 and FM2 were monitored and recorded during each sweep in order to assess the influence of axial flow through the journal clearance.

For the circumferential sweeps, the motion of the TPT is initiated at $\theta = 0$, which is located at 180 from oil inlet-1 shown on Fig. 3 (see also Fig. 6 AA), and proceeds clockwise 360°. Axially, the origin $Z = 0$, of the TPT is located in the oil bath at 4 mm to the left of the journal vertical wall, and the axial or longitudinal sweep is 45.7 mm to the right of the origin, (see also Fig. 6 AA).

The temperature and pressure measurements, as well as discussion of visual observations, are presented in the next section.

EXPERIMENTAL RESULTS

This section will present, in two separate parts, our experimental findings recorded during both the submerged journal start-up and steady-state modes. The steady-state experiments were conducted at three different journal speeds 209, 419, 628 rad/s (2000, 4000 and 6000 rpm).

The Start-up Regime

The study and discussion of the start-up behavior of the journal is of a qualitative nature rather than quantitative. The transient from 0 to 2000 rpm occurs extremely fast and the instruments and equipment at our disposal are designed to collect steady-state data rather than transient. However, a Fastax movie camera was used to record the incipient formation of the cavitation zone in both the upstream (convergent recompression and solution zone) and downstream (incipient nucelation zone) portions of the journal.

The four original frames and the corresponding overlays shown in Figs. 4(A)–(D), follow the stages of the formation of the cavity in its downstream section. Figures 4(A)–(C) show the bubble in the process of developing from individual gas (or vapor) nuclei which spread in the oil and form a cluster of bubbles which congregate to reach a critical radius and break the film homogeneity. As can be seen from the overlays, new small-bubble nuclei form at the periphery of the main bubble and they are then either engulfed in the larger gaseous (vaporous) structure or are carried downstream by the oil. This activity produces a rather unstable behavior of the boundary of the cavity. It becomes apparent that bubble formation is initiated at the point of lowest pressure around the minimum clearance region when the journal reaches an angular speed at which the cavitation pressure (P_g or P_v) is just attained. Many of the bubble nuclei will not grow and are swept downstream. They may then expand due to the decrease in pressure of the surrounding oil film and/or because new gaseous nuclei join them. The development of the cavitation zone during this initial transient stage we shall classify as pseudocavitation.

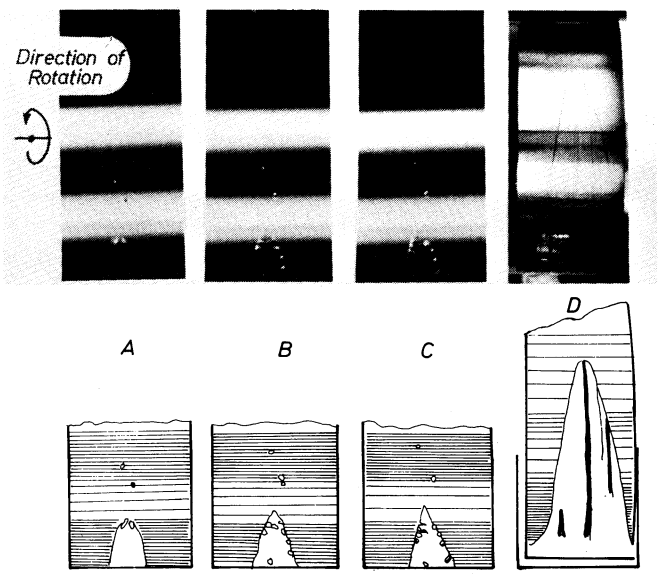

Fig. 4—Cavitation inception and development during journal start-up transients; the downstream section.

As the journal velocity increases, the pressure drops even further below P_g in the vicinity of the minimum clearance while downstram regions drop to P_g. Thus, a sustained process of gas release occurs throughout the divergent section enabling the bubbles to grow through a process of mass addition and coalescence. The apex of the bubble extends into the film up to the point where the pressure in the oil film is $P_f > P_g$. Thus, the process of true gaseous (and possibly vaporous) cavitation replaces the pseudocavitation at the end of the transient. Figure 4(D) shows the form of the cavity during the steady-state regime for a journal rotation of 2000 rpm.

Figures 5(A) through 5(F) spectacularly show the appearance and development of the gaseous phase in the form of a fern-leaf structure in the upstream region of the cavitation zone. The rather different shape of the bubbles is probably due to a combined effect of the normal and shear stresses produced by the flow pattern, bubble nuclei, and the pressures which characterizes the geometry in the vicinity of the minimum clearance. Figures 5(E), (F) show the more structured finger-like pattern of the final stages of the transient. It is worth noting here that finger-like structures are characteristic of the entire cavitation zone in the steady-state mode, even though Figs. 4 and 5 show much different patterns for the incipient transient in the upstream and downstream zones.

The Steady-state Regime

During the steady-state experiments, we have made both visual photographic records of the cavitation zone and quantitative measurements of the pressures and temperatures associated with it. The experiments have been run at 2000, 4000, and 6000 rpm, first with air dissolved in the oil (synthetic type) at atmospheric pressure and then at 4000 rpm with carbon dioxide-saturated oil at a reservoir pressure of 0.122 to 0.136 MPa (3 to 5 psig).

Figure 6 shows the downstream cavitation zone (gaseous air) at 2000 and 6000 rpm, respectively, while the TPT sensor performs a 360° rotation around the journal. It is evident from the photograph that as the angular velocity increases, low pressure ($P_g < P_f$) penetrates further and fur-

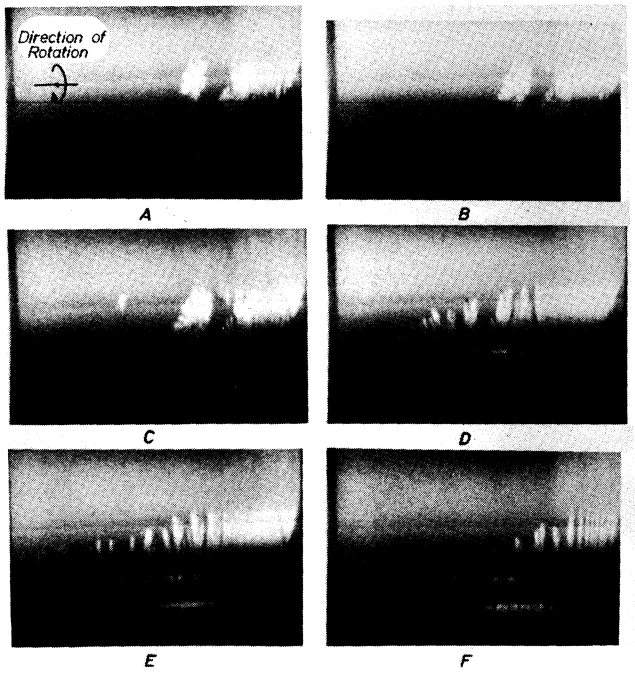

Fig. 5—Cavitation inception and development during journal start-up transients; the upstream section.

ther away downstream, allowing an extension of the cavitation zone. It is noteworthy that at 6000 rpm the shear forces apparently become sufficiently high to form a cloud of gas bubbles at the tip of the cavity or convergence zone. Many of the gas bubbles in the separation zone are not recompressed or redissolved into the oil, but are torn away and entrained towards the oil exit ports. These same effects (see also the motion-picutre supplement) are also observed at 2000 and 400 rpm, but with less intensity. The photographic evidence seems to provide credence to the physical aspects of the separation theory, as described in (*6*)–(*9*).

The pressure and temperature measurements presented in Figs. 7–10, were taken by the TPT, thus ensuring total spatial correspondence between the two sets of data. The curves of Figs. 7 and 8 have been obtained by first positioning the TPT at a given angle with respect to $\theta = 0$ (see also Fig. 6AA) and then performing a sweeping axial motion.

The oil reservoir, which feed the pump, had a bulk temperature of 18–19°C and was exposed to atmospheric pressure. The oil leaving the pump and reaching the submerged journal oil bath was at a pressure of approximately 0.172 MPa and temperatures ranging from 25 to 35°C.

The Pressure Measurements

Figure 7 details the pressure development along the Z axis, having θ as a parameter. The solid lines represent experiments done under atmospheric pressure with only air dissolved in the oil. The dashed line represents the pressure behavior under pressurization with carbon dioxide.

During the experiments, the total mass flow of oil has been maintained constant, thus assuring that little or no influence will be exerted by the mass flow on the pressure (or temperature) behavior. It follows that the variation in pressures was directly and solely influenced by the spatial coordinates of the TPT and the angular speed. It appears that at 2000 rpm subatmospheric pressure was not reached anywhere along the circumference, the pressure ranging from 0.137 to 0.13 MPa. As the velocity is increased to 4000 and to 6000 rpm, the regions of minimum pressure drop from above atmospheric to pressures ranging from 0.08 to 0.034 MPa at 4000 and 6000 rpm, respectively. Connecting these results to the photographic evidence of Fig. 6, one can understand and explain the extension of the cavitation zone as a function of the drop in pressures. Two more observations are important here. The first pertains to the variation of the pressure in the cavity region. This variation takes place both circumferentially and longitudinally. The explanation seems to reside in the fact that we have a small axial mass flow simulating seal leakage behavior. Figure 9 gives both a three-dimensional view and contour maps of the pressure envelope around the journal. The Z-θ plane shown in Fig. 9 is located at atmospheric pressure; its intersection with the pressure dome clearly delineates zones of minimum pressure. These zones are most prone toward producing hydrocarbon vapors. It becomes visually explicit that after the pressure reaches a minimum, it starts to rise in order to reach full oil film pressure at the apex of the cavity (convergence zone), thus maintaining continuity of the pressure profile. Figure 7 shows that the maximum pressure occurs immediately ahead of the 90° location with the minimum clearance located at approximately $\theta = 70°$. This corroborates the pressure profiles given by separation theory and that of Floberg, (*11*), (*12*). Figures 9 (A)–(C) also put in evidence the development of the subatmospheric pressure as a function of increasing angular speed, and the spatial location of the gaseous phase.

The Temperature Measurements

The methodology of recording the temperatures has been the same for both pressures and temperatures. Figures 8 and 10 give a parametric description and three-dimensional envelopes, respectively. It can be seen from the inspection of Fig. 8 that angular velocity, as it is varied from 2000 to 6000 rpm, contributes to the increase in temperature of the oil film and of the gaseous phase. Since mass flows are maintained constant and the viscous dissipation increases, it is expected that temperatures will increase. It is our belief that a combination of the lowest pressure and the highest temperature, as they are presented in the graphs, can contribute to hydrocarbon vapor release which, in fact, would amount to boiling of the oil. However, our spectrographic analysis revealed only very small traces of hydrocarbons in the gaseous samples and, due to the sampling technique, it would be hard to decide whether the hydrocarbon traces are due to released hydrocarbon vapors or to oil contamination of the gas sample.

Figure 10 shows the spatial distribution of temperatures in the θ and Z directions. In Figs. 10(A), (B), and (C), the reference plane Z-θ is at 20°C. The contour maps show the lines of constant temperature and help form a complete image of the development of the temperature envelope around the journal. The temperatures vary as the sensor passes through an array of alternating oil and gas streamers,

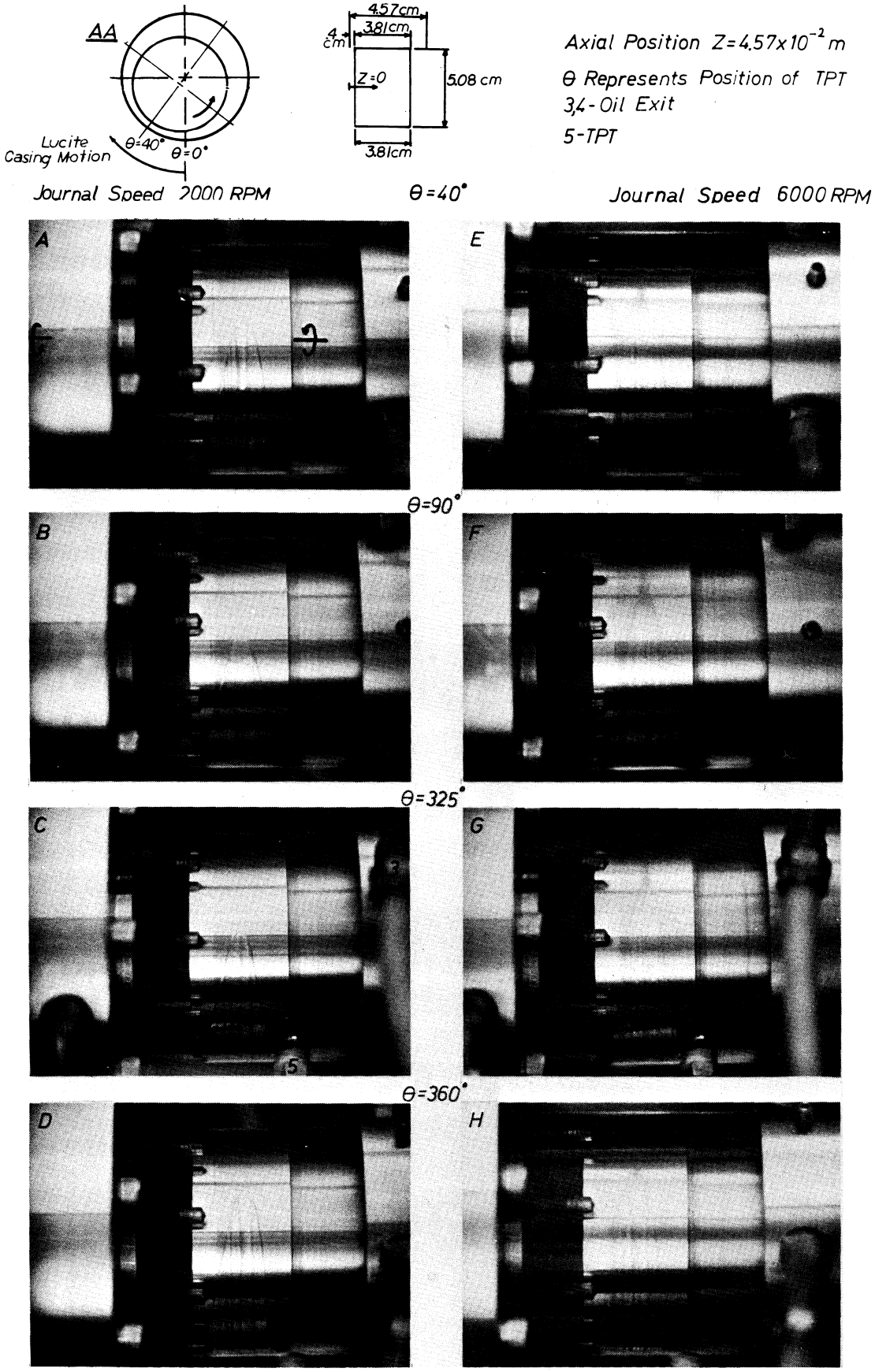

Fig. 6—Steady-state cavitation downstream representation at 2000 and 6000 rpm

the temperature in the gaseous phase being slightly different than that in the cooled oil.

CO_2 Pressure and Temperature Measurements (4000 rpm). For comparison purposes, a set of pressure and temper-

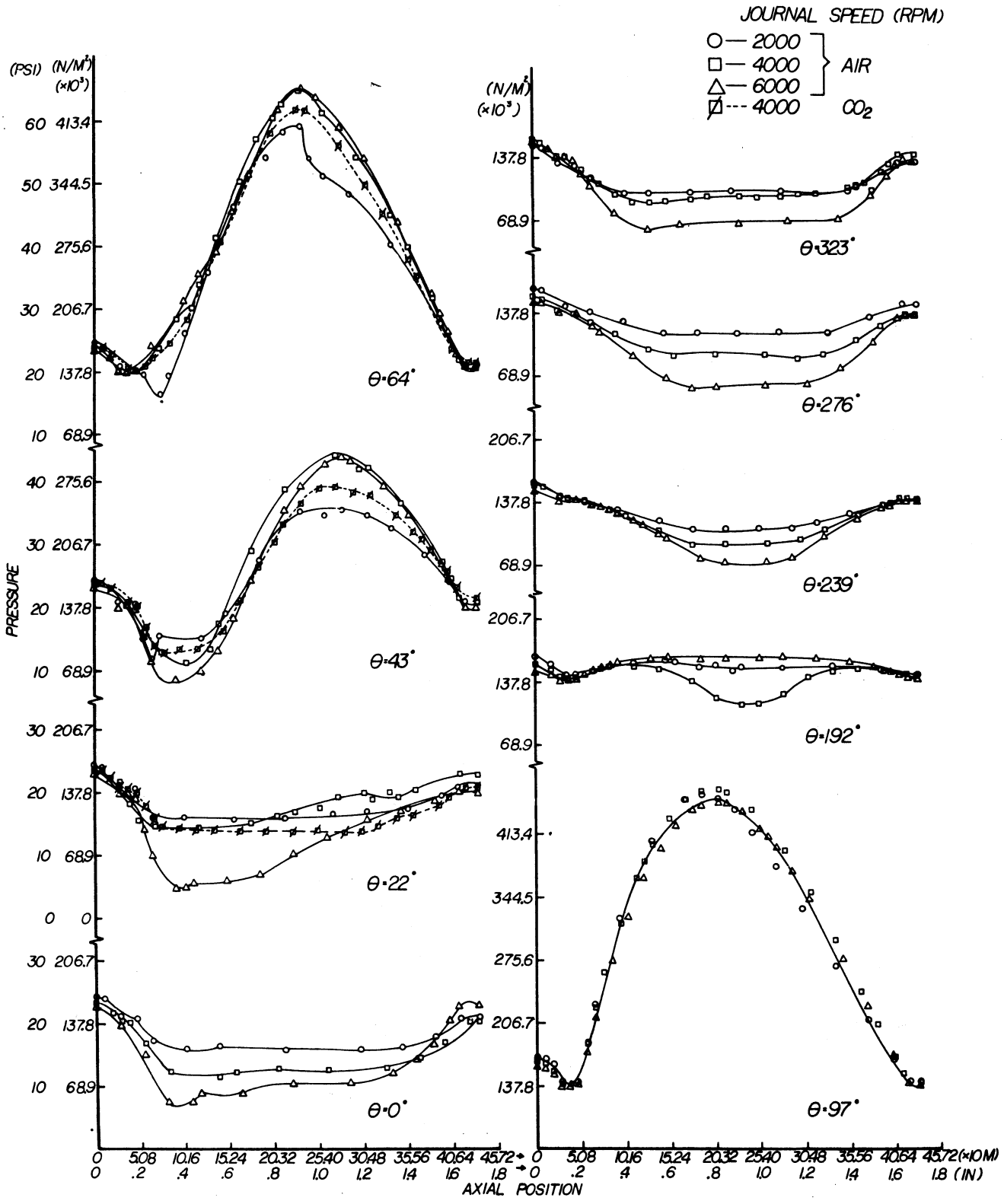

Fig. 7—Steady-state journal bearing pressure distribution as a function of TPT angular position

ature measurements have been taken while the oil reservoir, "Res" (Fig. 3), was saturated with CO_2 at 0.122 MPa (17.7 psia). Figure 11 presents a set of 3-D graphs and contour plots for both pressure and temperature. If the pressure reference plane, which is drawn at 0.1 MPa (14.7 psia) would be shifted by 0.021 MPa (3 psi), one would notice that the extent of the cavitation zone in the case of CO_2 is larger than that of the corresponding cavitation zone when the oil was saturated with air. This is due to the larger solubility in oil of CO_2 when compared with the solubility of air in oil. Data presented in the Appendix seem to support these experimental findings. Figure 12 presents a comparison of the contour plots of Fig. 9 and Fig. 11. Since absolute pressures in the CO_2 experiment are somewhat higher than in the air case, it appears that the CO_2 gas release temperatures must follow the trend as shown in Fig. 12(B).

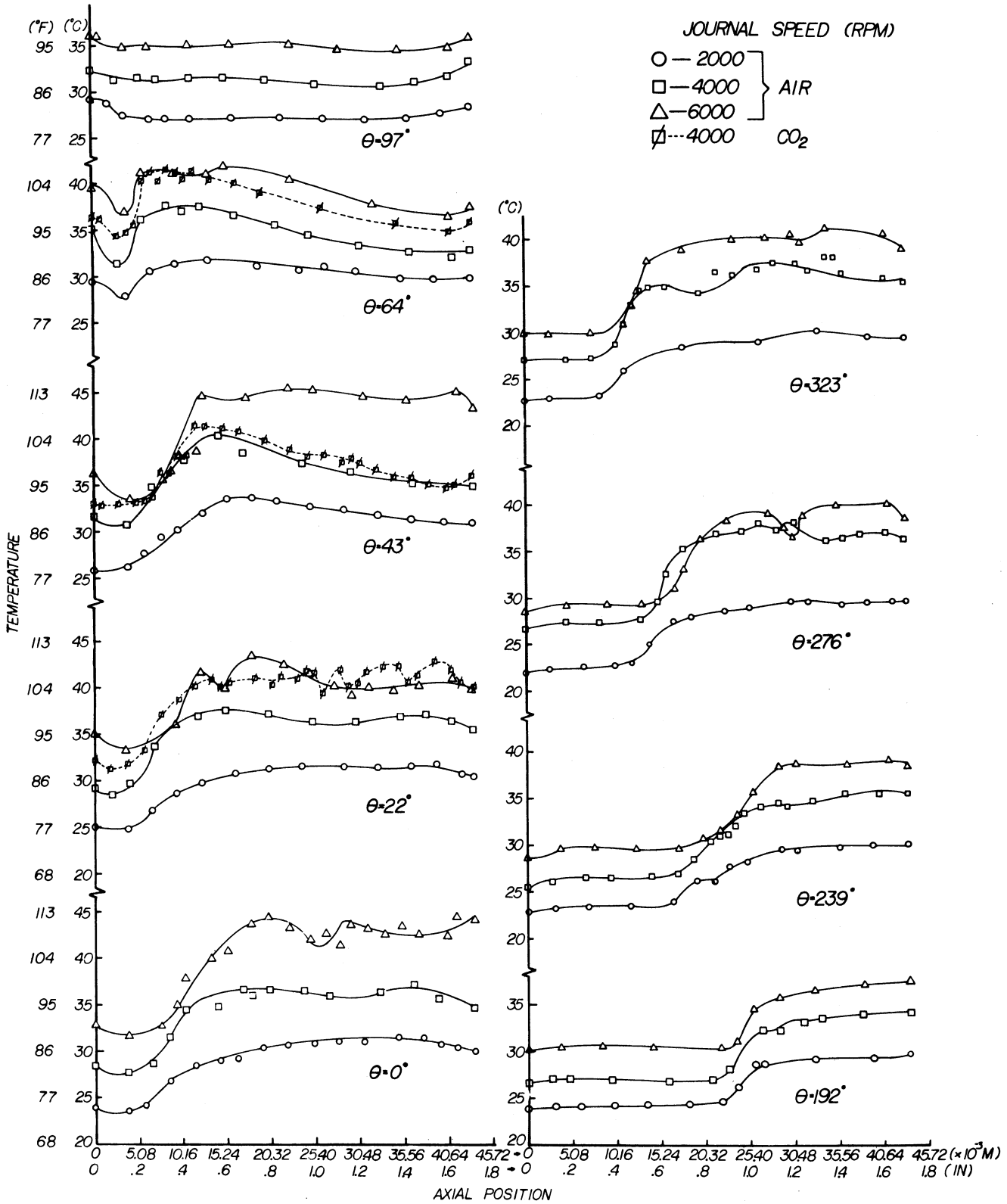

Fig. 8—Steady-state journal bearing temperature distribution as a function of TPT angular position

SUMMARY OF RESULTS

The experimental information presented herein has been reduced and analyzed in order to obtain three-parameter (3-D) plots and contour maps of pressure and temperatures around a fixed-position journal rotating within an eccentric lucite housing. To complement these results, a visual study was carried out to describe the inception and development of the cavity about the nonloaded journal (the only load being gravity) from transient to the characteristic finger-shape state. We have discussed the dilemma of the gaseous vs pseudo- or vaporous-cavity formation, and with the visual evidence along with the experimental curves of pressure

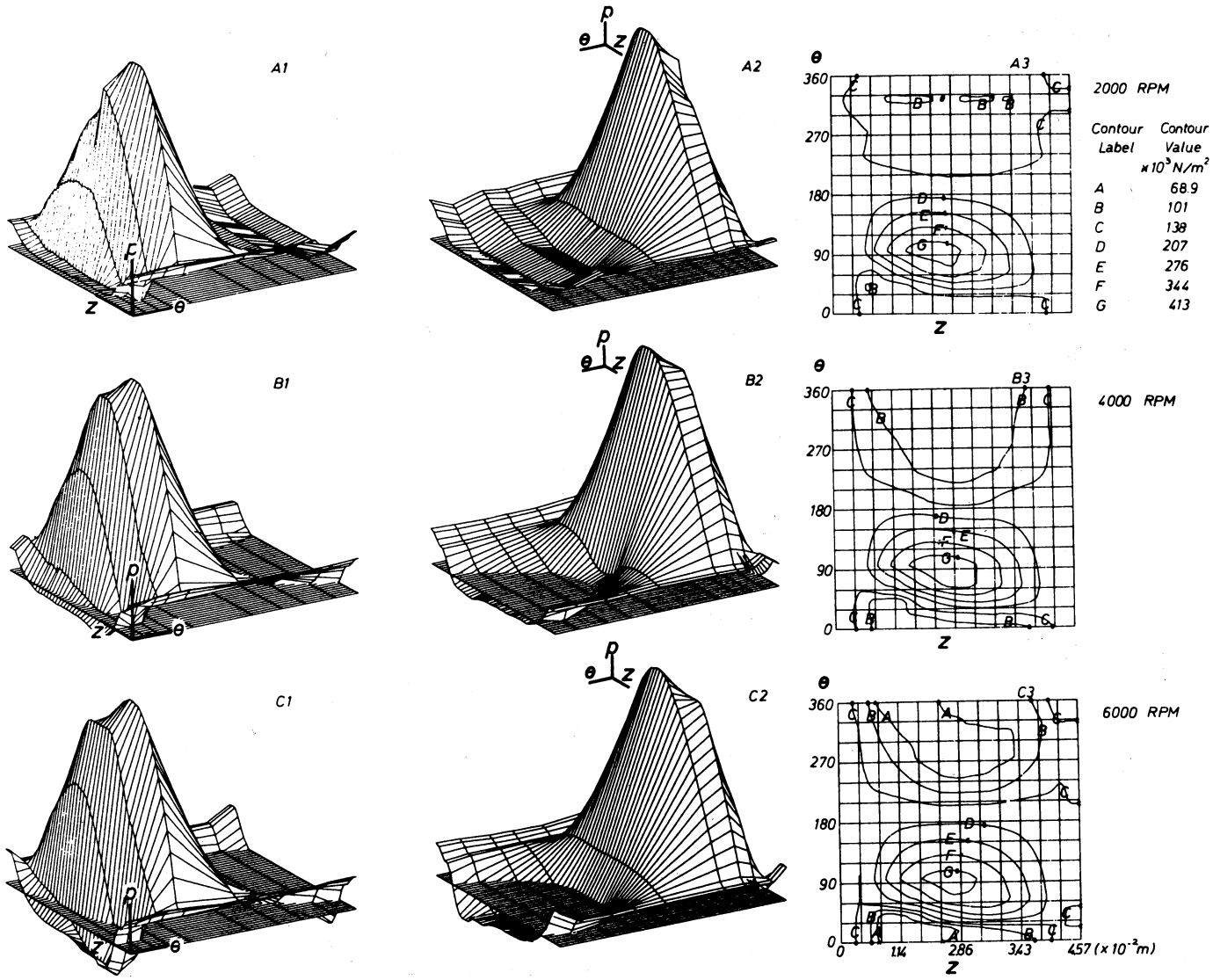

Fig. 9—3-D steady-state journal bearing pressure envelopes and contour maps; air in oil

and temperature have attempted to determine which of the three cavitation condition models (Swift-Stieber, separation, Floberg) are closer to reality. It seems from the data gathered that the Floberg pressure profile, Fig. 1, comes closer in shape to the profiles we are presenting. The development of subatmospheric pressures in the cavity are confirmed and it is quite apparent that these pressures drop as the angular velocity is increased. When the journal is rotating at 209 rad/s (2000 rpm), the cavity pressures are above atmospheric; however at 628 rad/s (6000 rpm), we have registered approximately a 0.0689 MPa (10 psia) drop in pressure below atmospheric.

The three-parameter (3-D) experimental pressure map is a new capability which helps visualize regions of peak and lowest pressures about the journal. The same capability has been added for temperatures and we intend in a follow-up paper to use the combination of pressures and temperatures in order to analytically confirm the nature of the cavity content and the mechanism of its formation.

It is worthwhile stressing the fact that the slight axial flow occuring between the journal and the lucite casing has created the simulated conditions of seal leakage, and thus we believe that the results obtained are beneficial to both the seal and journal bearing technology.

Finally, in the light of the discussion presented in the Appendix, it becomes increasingly apparent that, primarily, the cavity is filled with air-like gases. The appearance of hydrocarbon vapor in a cavity can be envisioned only as a result of extremely low pressures. Such pressures can be produced either by creating a vacuum on the free surface or by subjecting a fluid to a rapidly applied tensile or shear load, which can "fracture" the liquid along a surface determined by impurity sites (gas nuclei) in a fashion similar to the fracturing process in a solid.

ACKNOWLEDGMENTS

The authors want to thank H. Kistenmacher, Linde AG, Munich FRG and Glenn Atwood, University of Akron, Akron, Ohio, for their discussions and clarifying comments.

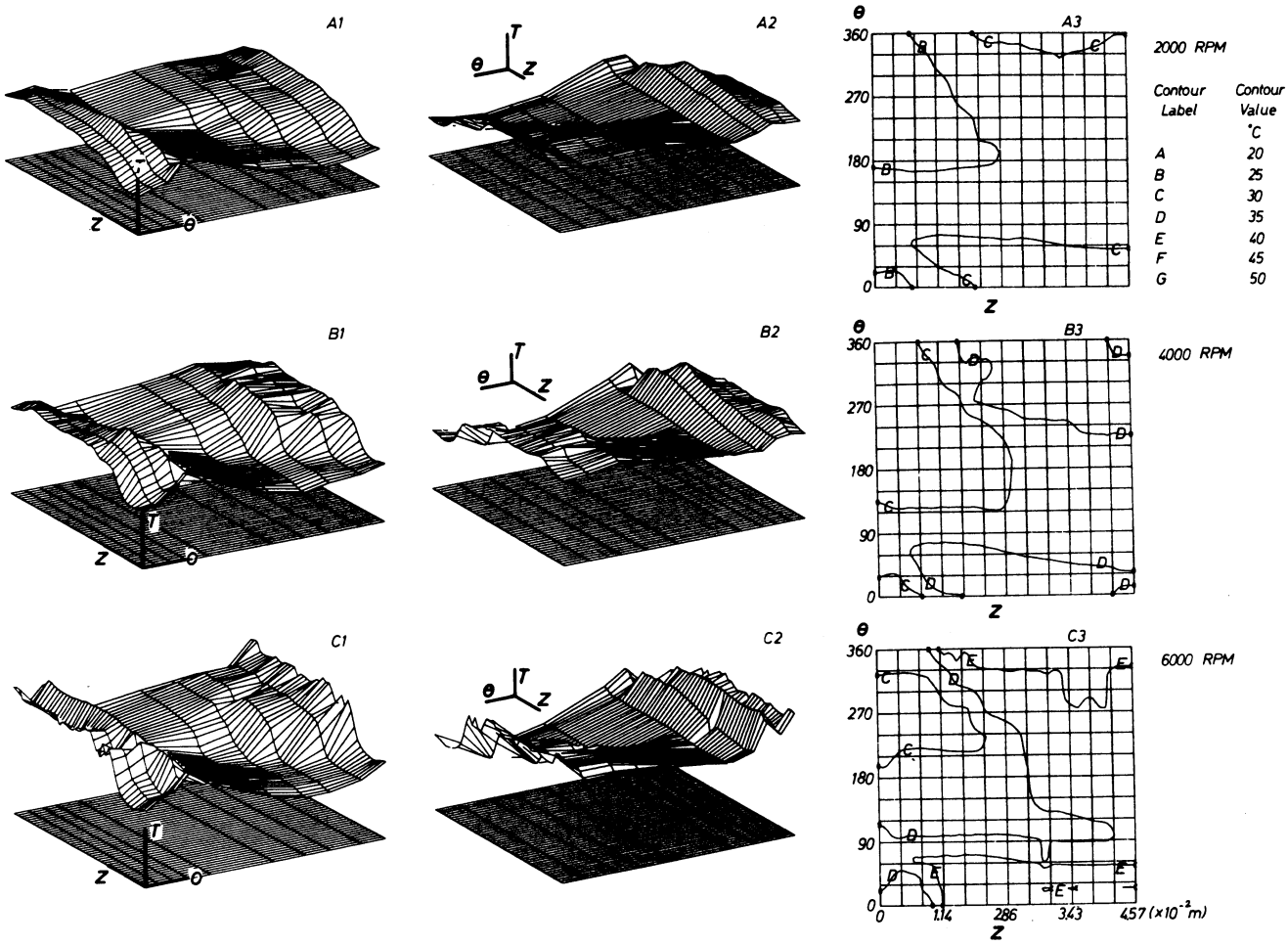

Fig 10—3-D steady-state journal bearing temperature envelopes and contour maps; air in oil

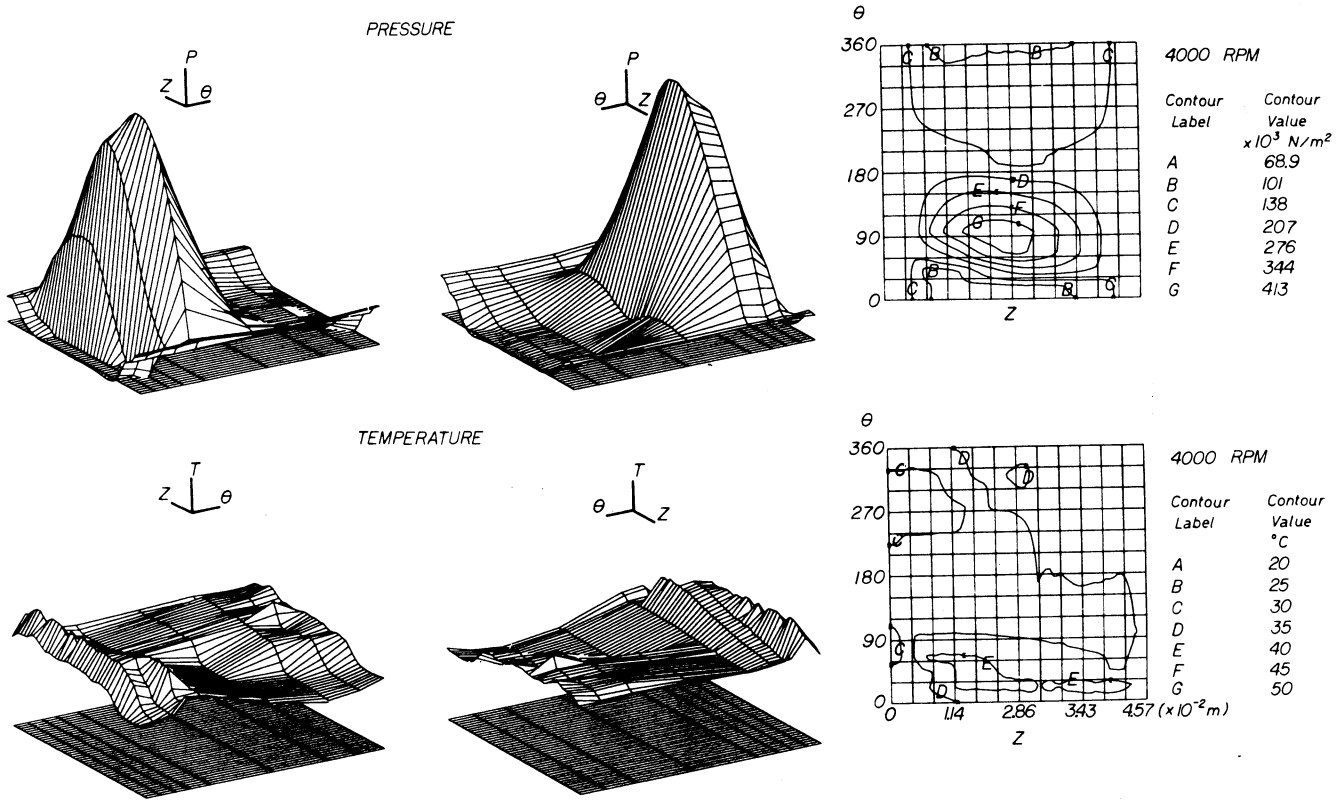

Fig. 11—3-D steady-state journal bearing temperature and pressure envelopes and contour maps; CO2 in oil

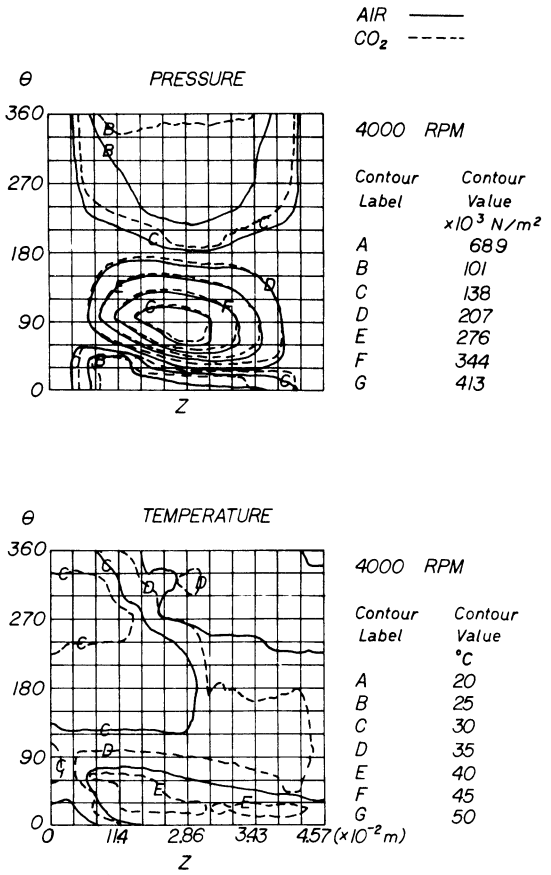

Fig. 12—Air and CO2 in oil, pressure and temperature contour maps comparison.

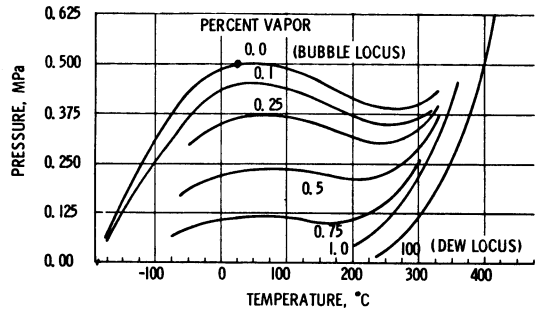

Fig. 13—Typical pressure temperature diagram for gas solubility in oil (C_{17}) as determined from single flash calculations.

REFERENCES

(1) Reynolds, O., "On the Theory of Lubrication and its Application to Mr. Beauchamps Tower's Experiments Including and Experimental Determination of the Viscosity of Olive Oil," *Phil. Trans. Roy. Soc.*, **177** (1886).

(2) Sommerfeld, A., "Zur Hydrodynamische Theorie der Schmiermittelreibung," *Z. Math. Phys.*, **50** (1904).

(3) Gumbel, L., *Monatsblatter Berlin Bezirksver*, VDI, **5** (1914).

(4) Swift, H. W. "The Stability of Lubricating Films in Journal Bearings," *Proc. Inst. Civil Engrs.* (London), **233** (1932).

(5) Stieber, W., *Das Schwimmlager*, VDI, (1933), Berlin.

(6) Hopkins, M. R., "Viscous Flow Between Rotating Cylinders and a Sheet Moving Between Them," *Brit. J. Appl. Phys.*, **8** (1957).

(7) Bretherton, F. P., "The Motion of Long Bubbles in Tubes," J. *Fluid Mech.*, **9,** pp 218–224 (1960).

(8) Taylor, G. I., "Cavitation of Viscous Fluid in Narrow Passages," J. *Fluid Mech.*, **16,** pp 595–619 (1963).

(9) Coyne, J. C. and Elrod, H. G., "Conditions for the Rupture of a Lubricating Film, Part I: Theoretical Model," *J. Lubr. Tech.*, **92,** pp 451–456.

(10) Cox, B. G., "An Experimental Investigation of the Stream Lines in Viscous Fluid Expelled form a Tube," *J. Fluid Mechanics,* **20,** pp 193–200 (1964).

(11) Floberg, L., "On Hydrodynamic Lubrication with Special Reference to Sub-cavity Pressures and Number of Streamers in Cavitation Regions," *Acta Polytechnica Scandinavica,* ME, Series 19, pp 1–35 (1965).

(12) Floberg, L., "Sub-cavity Pressures and Number of Oil Streamers in Cavitation Regions with Special Reference to the Infinite Journal Bearing," *Acta Polytechnica Scandinavica,* ME, Series 37, pp 1–36 (1968).

(13) Etsion, I. and Ludwig, L. P., "Observation of Pressure Variation in the Cavitation Region of Submerged Journal Bearings," NASA TM 81582, 1981.

(14) Hsu, Y. Y., "On the Site Range of Active Nucleation Cavities on a Heating Surface," *J. Heat Transfer,* **84C**(3), pp 207–216 (1962).

(15) Hsu, Y. Y. and Graham, R. W., "An Analytical and Experimental Study of the Thermal Boundary Layer and Ebullition Cycle in Nucleate Boiling, NASA TND-594, 1961.

(16) Bergles, A. E. and Rohsenow, W. M., "The Determination of Forced Convection Surface-Boiling Heat Transfer," *J. Heat Transfer,* **86C,** pp 365–372 (1964).

(17) Jacobson, B. O. and Hamrock, B. J., "High Speed Motion Picture Camera Experiments of Cavitation in Dynamically Loaded Journal Bearings," NASA TM-82789, 1981.

(18) Kistenmacher, H.: Linde, AG, Munich FRG, Private Communication.

APPENDIX

Flash Calculations to Determine the Solubility of Gas (Air) in Oil (C17)

Single flash calculations, using the Soave method (*18*) have been used in an attempt to justify the viewpoint put forward in this paper.

Figure 13 and the accompanying Table 1, are the result of these calculations. Figure 13 gives the percentage of the gas mixture released from an oil solution at a given temperature and pressure. With the help of Table 1, one can determine, based on the position on the liquid-vapor curve (Fig. 13), what is the actual composition of the gas mixture which flashes out of the oil solution.

The data presented in the table were taken for flashing points at 0.05, 0.1, and 0.5 MPa at 25°C. One can now explicitly see the composition of the liquid and gas fractions released. At all pressures, the quantities of kilo-moles of nitrogen, oxygen, argon, and CO2 in the gas are significantly higher than that of *n*-heptadecane (C17). In other words, the content of the gas released was more like "air" than hydrocarbon vapors. As the pressure decreases, the vapor-liquid equilibrium constant K for N_2, O_2, Ar, and CO_2 increases markedly, indicating that the solubility and the amounts of the above-mentioned components in the liquid oil diminished greatly. In parallel, the amounts of *n*-heptadecane released with the gas starts increasing as the pressure decreases significantly below the 0.05 MPa line and one can see the composition of the gas released changing from air-like structure to hydrocarbon vapor.

The *n*-heptadecane oil (C_{17}) was used as a control fluid, and is much more volatile than the synthetic oil used in the experiments presented in this paper.

TABLE 1—SATURATED OIL FEED AND LIQUID-VAPOR FLASH COMPOSITIONS AND ACTIVITY CONSTANTS FOR PRESSURES OF 0.05, 0.1, AND 0.5 MPa AT 25°C.

COMPONENT NAME	FEED Kmols	LIQUID Kmols	VAPOR Kmols	K VALUE
	T = 25°c P = 0.5 MPa			
Nitrogen	0.6498347	0.5783169	0.7151496E-01	134.9110
Oxygen	0.3169256	0.2968714	0.2005186E-01	73.68898
Argon	0.1383062E-01	0.1295026E-01	0.8802979E-03	74.15950
Carbon Dioxide	0.1938509E-02	0.1909867E-02	0.2864233E-04	16.36143
N-Heptadecane	99.99997	99.99995	0.2148885E-07	0.2344388E-06
Total	100.9825	100.8900	0.9247661E-01	
	T = 25°C P = 0.1 MPa			
Nitrogen	0.6498347	0.1150717	0.5347407	602.7195
Oxygen	0.3169256	0.8965719E-01	0.2272503	328.7454
Argon	0.1383062E-01	0.3894745E-02	0.9935413E-02	330.8623
Carbon Dioxide	0.1938509E-02	0.1244915E-02	0.6935862E-03	72.26054
N-Heptadecane	99.99997	99.99995	0.7067883E-06	0.9167059E-06
Total	100.9825	100.2099	0.7726274	
	T = 25°C P = 0.05 MPa			
Nitrogen	0.6498347	0.5630137E-01	0.5935327	120.4198
Oxygen	0.3169256	0.4695885E-01	0.2699596	656.6794
Argon	0.1383062E-01	0.2038125E-02	0.1179245E-01	660.9146
Carbon Dioxide	0.1938509E-02	0.8570638E-03	0.1081440E-02	144.1323
N-Heptadecane	99.99997	99.99995	0.1572325E-05	0.1796036E-05
Total	100.9825	100.1061	0.8763721	

1. Report No.	2. Government Accession No.	3. Recipient's Catalog No.
NASA TM-82996		

4. Title and Subtitle	5. Report Date
EXPERIMENTAL INVESTIGATION OF THE VAPOROUS/GASEOUS CAVITY CHARACTERISTICS OF AN ECCENTRIC JOURNAL BEARING	October 1982
	6. Performing Organization Code: 505-32-42
7. Author(s): M. J. Braun and R. C. Hendricks	8. Performing Organization Report No.: E-1429
	10. Work Unit No.
9. Performing Organization Name and Address: National Aeronautics and Space Administration, Lewis Research Center, Cleveland, Ohio 44135	11. Contract or Grant No.
	13. Type of Report and Period Covered: Technical Memorandum
12. Sponsoring Agency Name and Address: National Aeronautics and Space Administration, Washington, D. C. 20546	14. Sponsoring Agency Code

15. Supplementary Notes: M. J. Braun, University of Akron, Akron, Ohio 44325 and R. C. Hendricks, NASA Lewis Research Center. Prepared for the Joint Lubrication Conference cosponsored by the American Society of Lubrication Engineers, Washington, D. C., October 4-6, 1982.

16. Abstract

17. Key Words (Suggested by Author(s))	18. Distribution Statement
Cavitation Seal Bearing Eccentric seal Eccentric bearing	Unclassified - unlimited STAR Category 34

19. Security Classif. (of this report)	20. Security Classif. (of this page)	21. No. of Pages	22. Price*
Unclassified	Unclassified		

* For sale by the National Technical Information Service, Springfield, Virginia 22161